Whole metagenome profiling reveals skin microbiome-dependent susceptibility to atopic dermatitis flare

Kern Rei Chng[1], Angeline Su Ling Tay[2], Chenhao Li[1], Amanda Hui Qi Ng[1], Jingjing Wang[3,4,5], Bani Kaur Suri[6], Sri Anusha Matta[6], Naomi McGovern[7], Baptiste Janela[7], Xuan Fei Colin C. Wong[2], Yang Yie Sio[6], Bijin Veonice Au[3], Andreas Wilm[1], Paola Florez De Sessions[1], Thiam Chye Lim[8], Mark Boon Yang Tang[9], Florent Ginhoux[7], John E. Connolly[3,5,10], E. Birgitte Lane[2], Fook Tim Chew[6], John E. A. Common[2]* and Niranjan Nagarajan[1]*

Whole metagenome analysis has the potential to reveal functional triggers of skin diseases, but issues of cost, robustness and sampling efficacy have limited its application. Here, we have established an alternative, clinically practical and robust metagenomic analysis protocol and applied it to 80 skin microbiome samples epidemiologically stratified for atopic dermatitis (AD). We have identified distinct non-flare, baseline skin microbiome signatures enriched for *Streptococcus* and *Gemella* but depleted for *Dermacoccus* in AD-prone versus normal healthy skin. Bacterial challenge assays using keratinocytes and monocyte-derived dendritic cells established distinct IL-1-mediated, innate and Th1-mediated adaptive immune responses with *Staphylococcus aureus* and *Staphylococcus epidermidis*. Bacterial differences were complemented by perturbations in the eukaryotic community and functional shifts in the microbiome-wide gene repertoire, which could exacerbate a dry and alkaline phenotype primed for pathogen growth and inflammation in AD-susceptible skin. These findings provide insights into how the skin microbial community, skin surface microenvironment and immune system cross-modulate each other, escalating the destructive feedback cycle between them that leads to AD flare.

Atopic dermatitis (AD; OMIM 603165) is a dry, itchy, inflammatory skin disorder that affects up to 20% of the population in developed countries[1,2]. AD is cyclical, with relapsing flare periods that induce cutaneous phenotypes and non-flare periods with intact skin and no overt clinical signs of infection[3].

Multiple genetic risk factors for AD have been identified, highlighting the specific importance of innate and adaptive immune pathways and skin barrier function[4]. The strongest risk factor for AD is loss-of-function mutations in the gene encoding filaggrin (*FLG*)[5–7], a key component of terminal differentiation and skin barrier function including pH regulation and epidermal hydration[8]. Human studies and *in vitro* experiments have shown that presence of Th2 cytokines can also perturb skin barrier function via multiple mechanisms including downregulation of antimicrobial peptides[9], increased expression of serine proteases[10], downregulation of keratinocyte differentiation[9,11] and expression of profilaggrin processing enzymes[12]. This complex interplay between the immune system and direct or indirect barrier dysfunction creates a skin microenvironment where percutaneous sensitization can contribute to atopic disease[13–16].

Skin infections are a frequent problem encountered by AD patients, with bacterial colonization by *Staphylococcus aureus* observed on both lesional and non-lesional skin[17], and treatment with antibiotics or dilute bleach baths often being successful[18].

Strong perturbation of the skin microflora during flares, including massive reduction in microbial diversity has also been demonstrated[19]. Antigen transfer through a defective skin barrier can influence host immunity and, in turn, the host immune system can shape the microbiome. For instance, skin microbiome variations have been linked to primary immunodeficiency diseases with AD-like presentation[20], highlighting that alterations in immunity can drive microbial dysbiosis. The clear differences observed in microbiome composition between dry, oily and moist body sites in healthy skin[21] suggest that conditions affecting the skin microenvironment will also have profound effects on the microbiome, even in asymptomatic states. Thus, while current data strongly indicate a significant role for the skin microbiome in AD pathogenesis, the potentially protective or predisposing role of inter-flare microbiota remains to be explored.

In this study, high-throughput whole-metagenome sequencing was used to explore between-flare skin flora in a volunteer cohort epidemiologically stratified for AD[22]. This was based on the hypothesis that, by examining non-flare conditions when the disease is dormant but the individual is still AD-susceptible, new insights into the role of the microbiome in AD disease pathogenesis can be determined. Molecular indicators of skin health are difficult to define, and predicting early signs of susceptibility to skin disease would enable early intervention and better outcomes. Skin microflora

[1]Genome Institute of Singapore, Singapore 138672, Singapore. [2]Institute of Medical Biology, Singapore 138648, Singapore. [3]Institute of Molecular and Cell Biology, Singapore 138673, Singapore. [4]Department of Neurology, The First Affiliated Hospital of Zhengzhou University, Zhengzhou, Henan 450001, China. [5]Institute of Biomedical Studies, Baylor University, Waco, Texas 76798, USA. [6]Department of Biological Sciences, National University of Singapore, Singapore 117543. [7]Singapore Immunology Network, Singapore 138648, Singapore. [8]Division of Plastic, Reconstructive & Aesthetic Surgery, National University Health System, Singapore 119074, Singapore. [9]National Skin Centre, Singapore 308205, Singapore. [10]Department of Microbiology and Immunology, National University of Singapore, Singapore 117545, Singapore. *e-mail: nagarajann@gis.a-star.edu.sg; john.common@imb.a-star.edu.sg

in asymptomatic, high-risk individuals was compared to a control group to enrich for differences that predispose or protect individuals from flares. Significant bacterial and eukaryotic variations were observed in skin microbial composition between control and AD-prone groups. Experimental characterization using immune challenge assays and functional analysis of microbial pathways identified a pathogenic niche that is primed for switch to flares, highlighting the potential functions of the inter-flare microbiome in AD.

Results

Establishing a robust and convenient skin microbiome analysis protocol. A selection of widely used skin sampling and microbiome profiling approaches were evaluated, complementing earlier work based on marker genes[23], but with a specific focus on whole-metagenome analysis. Three sampling methods were compared: (1) skin swabbing (http://hmpdacc.org/) ('swab'), (2) a modified cup scrub ('cup scrub') and (3) a tape-stripping technique that has not been evaluated for metagenomics ('tape'). All sampling approaches were combined with two profiling approaches: (1) amplification and sequencing of 16S rRNA gene ('16S') and (2) shotgun whole-metagenome sequencing and analysis of total DNA ('WM'). Samples were collected from left and right antecubital fossae (Ac) and retroauricular crease (Ra) of three healthy volunteers to assess their distinctness and/or concordance as a measure of the reproducibility of the results (Supplementary Table 1 and Supplementary Fig. 1).

Overall, high concordance was observed between microbial abundance profiles derived for left and right Ac from various sampling approaches ($r > 0.86$; Supplementary Fig. 2a). Higher concordance was also observed using whole-metagenome profiles ($r > 0.95$) versus 16S ($r > 0.86$), and slightly higher concordance using tapes as opposed to swab or cup scrub. Slight biological differences between left and right Ac were also consistently captured across sampling approaches. Given the concordance between sampling approaches, the tape-based protocol stands out for its ease of use in a clinical setting (see Methods) and robustness for DNA collection (Supplementary Fig. 1).

Lower concordance was observed between profiling approaches due to the inherent differences in experimental and analytical procedures (Supplementary Figs 2b and 3). However, whole-metagenome profiling showed higher internal consistency than 16S profiling (Supplementary Figs 2a,b and 3). Whole-metagenome sequencing also enabled analysis of eukaryota and viruses with high reproducibility (Supplementary Fig. 2c). Principal coordinates analysis of profiles from various sampling approaches readily reflected the distinctness of skin surface niches and demonstrated their separation from potential environmental contamination (Supplementary Fig. 2d).

The combination of tape sampling and whole-metagenome sequencing was validated as an easy-to-use and robust skin microbiome analysis protocol by applying it to 80 Asian skin microbiome samples. The success rate for sequencing libraries was >98.7%, despite challenges of sample collection in a clinical setting and the potential for low microbial biomass on skin surfaces, as noted previously[24] (Supplementary Fig. 4). Analysis of control samples confirmed that our sampling strategy was highly specific (Supplementary Figs 1 and 4).

Intra- and inter-individual variability in the skin microbiome of a cohort stratified for AD. Microbiome samples (tape) were collected from clinically intact, non-inflamed skin in 40 adult volunteers. Sampling left and right Ac provided a more robust individual Ac skin microbiome representation. The cohort was stratified into three groups defined according to the ISAAC study questionnaire[25]: (1) *AD case group*, with volunteers reporting past

AD episodes ($n = 19$; 1 library failed), (2) *Control group*, with volunteers who were skin prick test (SPT) negative and have no AD history ($n = 15$) and (3) *Skin prick test positive (SPT+) group*, with volunteers ($n = 5$) having no AD history but SPT+ (Supplementary Tables 2–4). The SPT+ group serves as a reference for individuals with atopy but not reporting AD. The three groups were approximately matched according to mean age (Control: 24.1; Case: 23.1; SPT+: 23.0), gender (Control: 8 males, 7 females; Case: 8 males, 12 females; SPT+: 3 males, 2 females) and ethnicity (Chinese) (Supplementary Table 2). Trans-epidermal water loss (TEWL) and pH measurements were collected to validate the skin health of sampled regions and no statistically significant differences between cases and controls were noted (Supplementary Fig. 5a).

Examination of the principal axes of variation in Ac microbiomes showed that all three groups clustered together with similar bacterial composition overall (Fig. 1a). Evaluating intra- (left versus right) and inter-individual variability across cohorts, we noted an individual-specific bacterial composition signature marked by higher intra-individual similarity ($P = 4.7 \times 10^{-10}$; Fig. 1b). These consistent individual-specific profiles were then averaged for robustness and compared across groups to characterize patterns of bacterial variation specific to inter-flare AD skin. Higher similarity in bacterial composition was observed within the case and SPT+ groups than compared to the control group ($P = 2.4 \times 10^{-6}$ and 2.8×10^{-4}, respectively; Fig. 1c), despite the absence of significant differences in bacterial diversity between groups (Supplementary Fig. 5b). A trend for lower bacterial diversity in subjects with *FLG*-null mutations ($n = 3$; two cases, one control) versus *FLG* wild-type volunteers ($n = 36$) was observed (but was not statistically significant; Supplementary Fig. 5c).

Defining a bacterial signature for susceptibility to AD. To characterize the distinctness of AD-associated microbiomes and establish a bacterial signature for AD susceptibility, we systematically compared non-flare, baseline profiles at the genus level (due to the limited resolution for some species; see Methods) across groups. Strong enrichment was observed for potential pathobionts belonging to the genera *Streptococcus* and *Gemella* in AD and SPT+ groups relative to the controls (FDR-adjusted $P < 0.05$, Wilcoxon rank-sum test; Fig. 1d, Supplementary Table 5), pointing to a role in sensitizing the immune system through the skin. The genus *Dermacoccus* was strongly depleted in the AD group relative to controls and SPT+ individuals (FDR-adjusted $P < 0.05$, Wilcoxon rank-sum test; Fig. 1d and Supplementary Table 5). *Dermacocci* belong to the order *Actinomycetales*, known for producing secondary metabolites with anti-inflammatory and anti-microbial properties[26]. In addition, we detected enrichment in the genera *Veillonella* and *Haemophilus*, as well as depletion in *Deinococcus* and *Methylobacterium*, in AD versus normal controls (Supplementary Fig. 6a and Supplementary Table 5). Canonical correlation analysis of taxonomic profiles and clinical information confirmed the predominant association of all seven identified genera with AD status ($\rho = 0.60$). Stratification by gender and cream usage showed significant differences in a subset and similar enrichment/depletion trends in all identified genera (Supplementary Fig. 6b,c). Interestingly, different genera were significantly differentially abundant in males versus females, potentially due to insufficient sample size or bonafide gender-specific differences. Patterns observed for SPT+ individuals reinforced the observations for the AD group, that is, enrichment in potentially sensitizing pathogens but no depletion of putatively protective bacteria, highlighting the distinct aetiology of this group.

At the species level, nine bacteria were identified to have significant AD-associated microbiome differences (Supplementary Table 5). Among these, three α-haemolytic *Streptococci* were
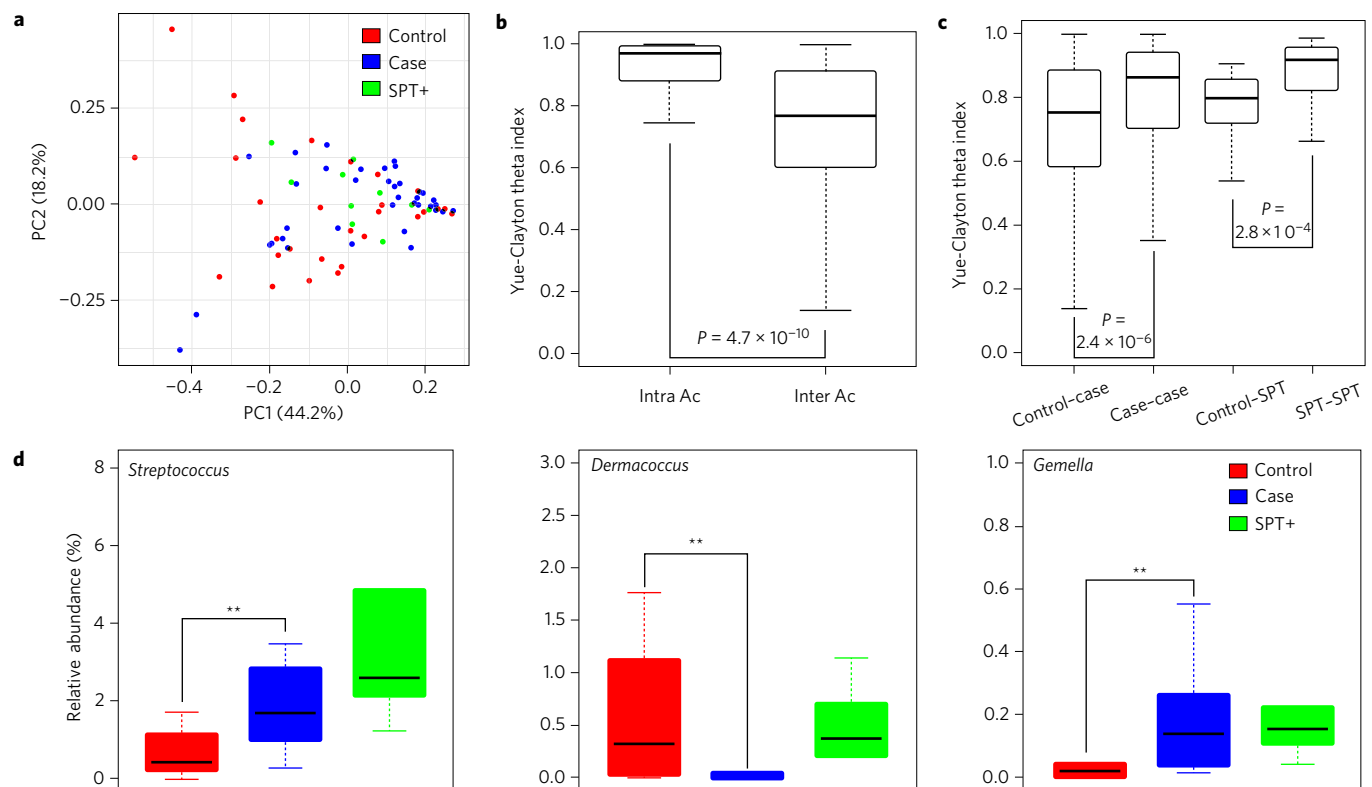
Figure 1 | Baseline bacterial diversity and signatures associated with AD. a, Principle coordinates analysis based on Bray–Curtis dissimilarity between skin microbiome profiles (genus level) for all volunteers in an epidemiologically stratified cohort. **b**, Box plot quantifying the similarity of the skin microbiome within (left and right Ac) and across individuals (genus-level profiles). **c**, Box plot quantifying the similarity of the skin microbiome within and across groups in the cohort (genus-level profiles). **d**, Box plots showing the relative abundances of the top three differentially abundant genera in AD patients ($n = 19$) relative to normal controls ($n = 15$). SPT+ refers to skin prick test positive non-AD volunteers ($n = 5$). All P values were calculated using the two-sided Wilcoxon rank-sum test. **FDR-adjusted $P < 0.05$. Box plot whiskers represent 1.5 × interquartile range or the maximum/minimum data point within the range.

enriched in AD subjects, but *S. pyogenes* (β-haemolytic), previously associated with severe skin infections[27], was not detectable in any subjects studied (Supplementary Fig. 7). The majority of species enriched in AD-susceptible subjects are known commensals or opportunistic pathogens of the oral cavity, the significance of which remains presently unclear (Supplementary Note 1 and Supplementary Table 5).

Correlation analysis to predict bacterial interactions in skin communities identified >142 interactions (Supplementary Note 2) including a known antagonistic relationship (negative correlation) between *P. acnes* and *S. epidermidis*[28], and a significant negative correlation between *Dermacoccus* and *Methylobacterium* species with *S. aureus* (see Methods; Supplementary Table 6). Agar-diffusion assays using bacteria identified here as enriched in AD non-flare skin, in competition with *S. aureus*, further support the hypothesis that interactions between these species have a functional role in AD (Supplementary Note 3 and Supplementary Fig. 8). Finally, the possibility of using a purely bacterial signature for stratifying various groups in our cohort was assessed. By restricting analysis to the most significant differentially abundant genera (*Streptococcus*, *Gemella* and *Dermacoccus*), we obtained robust consensus clustering of profiles into three distinct clusters (Supplementary Fig. 9; see Methods).

Strain-level differences in the AD-associated microbiome. A systematic approach to catalogue sequence variants was used to determine whether shifts in strain abundance correlated with AD susceptibility[29] (see Methods). We studied staphylococci and, in particular, *S. aureus*, because of its known AD association[17], predominance during flares and correlation with clinical severity[19]. An increased percentage of *S. aureus* carriers was noted in our AD

cohort over controls (Supplementary Fig. 10), showing that these differences are also present (albeit more subtly) on non-flare skin of AD-susceptible individuals. Overall, *S. epidermidis* exhibited greater strain diversity than *S. aureus* across cohorts (Supplementary Fig. 11a,b). An analysis of single nucleotide polymorphisms (SNPs) also indicated that important strain-level differences, including in key virulence factors, exist in distinct groups (Supplementary Table 7). For example, the AD group preferentially hosted a microbial population carrying a variant of the staphylococcal lipase gene *geh*, a well-characterized virulence factor[30,31], with a basic arginine residue (CGC) at amino acid position 373, rather than the polar threonine residue (ACC) (Supplementary Fig. 11c). This preferential polymorphism can modify the enzymatic efficacy of staphylococcal lipase and thus be positively selected for by the need to adapt to the AD-associated drier, lipid-reduced skin microenvironment. By analysing data from a recent study that sampled different human skin microbiomes[21], we reconfirmed this, noting a preference for the arginine residue (CGC) in dry (volar forearm, Vf) versus moist environments (Ac) ($P = 0.055$; Wilcoxon rank-sum test; Supplementary Fig. 11d).

AD-associated bacteria elicit distinct inflammatory and immune responses. To investigate the impact of bacterial populations identified from this study on non-flare AD versus normal skin, the capacity of microbial species to stimulate the immune system was examined. Six bacterial species (Supplementary Table 8) were selected, including a known skin pathogen (*S. aureus*) and a commensal (*S. epidermidis*) that have been shown to increase in abundance during flares[19]. *Deinococcus radiodurans* and *Dermacoccus nishinomiyaensis* were selected as representative skin
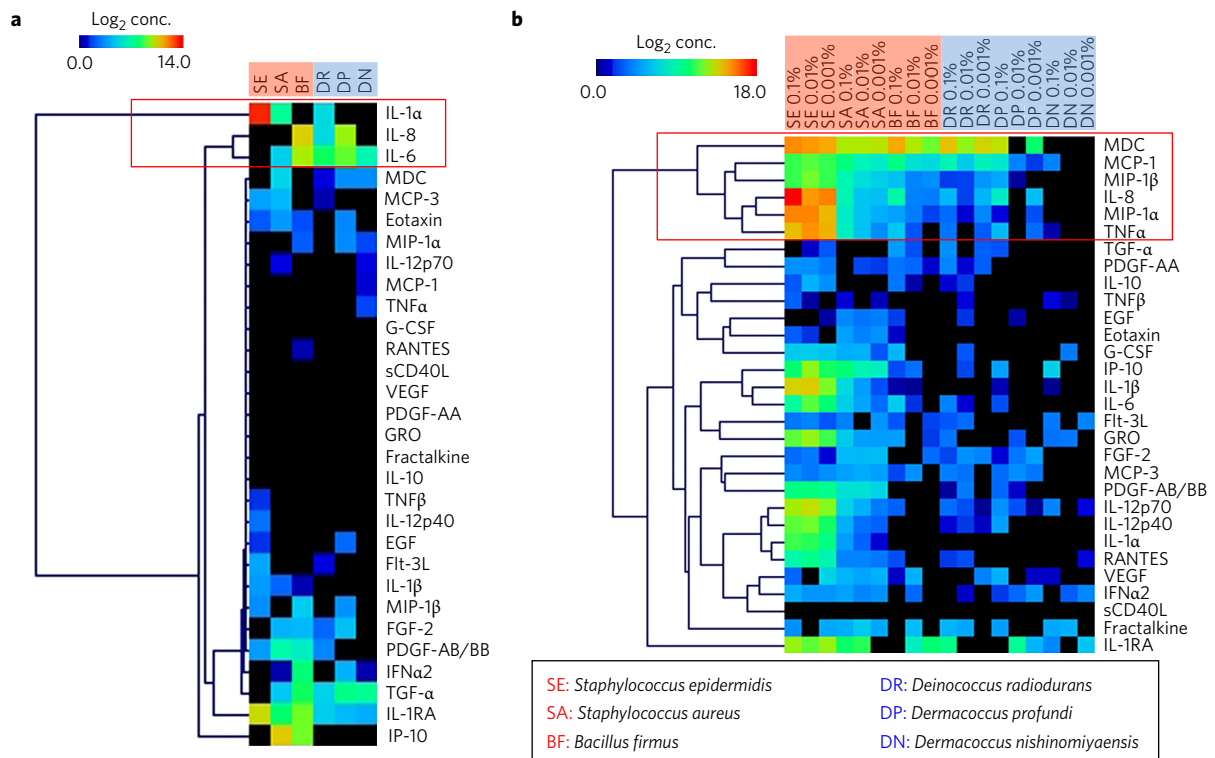
Figure 2 | Hierarchical clustering comparing cytokine secretion profiles of human keratinocytes and dendritic cells with various bacterial supernatants. a, Heat map representation of $\log_2$ average medium normalized cytokine secretion levels in human keratinocytes ($n = 3$) that were stimulated for 24 h with various bacterial supernatants. Cytokines associated with an IL-1α driven inflammation signature are boxed in red. Hierarchical clustering of cytokine profiles was performed using the Euclidean distance metric. **b**, Heat map representation of $\log_2$ average medium normalized cytokine secretion levels in human moDCs ($n = 3$) that were stimulated for 24 h with bacterial supernatants as indicated. Cytokines associated with a TNF-driven myeloid activating signature are boxed in red. Hierarchical clustering of cytokine profiles was performed using the Euclidean distance metric. SE, *S. epidermidis*; SA, *S. aureus*; BF, *B. firmus*; DR, *D. radiodurans*; DP, *D. profundi*; DN, *D. nishinomiyaensis*.

commensals of their genera (depleted in AD; Supplementary Table 5), *Dermacoccus profundi* as control non-skin commensal from its genus, and *Bacillus firmus* as non-commensal immunostimulatory positive control[32]. Human keratinocytes, moDCs as well as primary human and mouse Langerhans cells (LCs) were challenged with live bacteria and supernatants.

In human keratinocytes, a classical IL-1-driven inflammation signature of cytokines and innate immune response was induced by live bacteria (Supplementary Fig. 12a) and supernatants (Fig. 2a). Specifically, IL-1α increased strongly with challenge from *S. epidermidis* and *S. aureus*, while moderate induction of IL-1β was observed with *S. epidermidis*, *S. aureus* and *B. firmus* (Fig. 2a). In addition, specific chemokines known to play a role in the recruitment of granulocytes and DCs were stimulated, including IL-8 in *B. firmus* and *D. profundi*, and IP-10 in *S. aureus*, *B. firmus* and *D. profundi* (Fig. 2a and Supplementary Fig. 12b). The muted response of *D. nishinomiyaensis* (skin commensal) in comparison to *D. profundi* (non-skin commensal control) is noteworthy and supports the notion that a protective role for *Dermacoccal* species is likely to be specific to skin commensals. Overall, these data are consistent with the known cytokine profile that induces maturation of naive DCs[33] and supports the hypothesis that keratinocyte activation by *S. epidermidis* and *S. aureus* can lead to recruitment and stimulation of DCs in the skin.

Challenge assays with human and mouse primary LCs indicated that all bacteria elicit a muted response (Supplementary Figs 13 and 14), in agreement with previous results[34] and the complex roles played by LCs in skin[35]. Challenge of moDCs elicited a more pronounced and graduated immune activation response from different bacteria, with *Staphylococcal* species at one end of the spectrum

(most response) and *Dermacocci* at the other end (Fig. 2b and Supplementary Fig. 12c). *Staphylococcus epidermidis*, *S. aureus* and *B. firmus* induced a tumour necrosis factor (TNF) driven myeloid activating signature of cytokines and chemokines, with chemokine profiles predicted to recruit neutrophils and monocytes (Fig. 2b). We also noted induction of a Th1 polarizing cytokine signature (IL12p70 and IL12p40) in response to *S. epidermidis* and, to a lesser extent, *S. aureus*, *D. radiodurans* and *D. profundi*. Overall, our results suggest that *S. epidermidis* and *S. aureus* invoke a strong immune inflammatory response in an *in vitro* setting. In contrast, *D. radiodurans* and *D. nishinomiyaensis* elicit a muted response, supporting the hypothesis that the presence of skin commensal *Dermacocci* and *Deinococci* plays a protective role on skin.

Changes in the eukaryotic diversity on skin associated with AD.

Whole-metagenome analysis enables the characterization of eukaryotic and viral constituents of the microbiome, providing an opportunity to study their biological roles in AD. Overall, we observed higher relative abundance of eukaryotes in controls versus cases ($P = 0.0045$), but no statistically significant differences in bacterial ($P = 0.21$) and viral proportions ($P = 0.51$; Fig. 3a). Despite their relatively low density (Fig. 3a), a surprising diversity of viruses/phages was identified (Fig. 3b). As expected[21], these were dominated by phages, although a few viruses could also be readily detected (for example, human papillomavirus) with no significant differences observed between cohort groups (potentially due to low abundances).

Eukaryotic microbiome residents on human skin are dominated by the *Malasseziaceae* family (Fig. 4a), and these were clearly depleted in AD-susceptible individuals ($P < 0.01$, Wilcoxon rank-sum test;
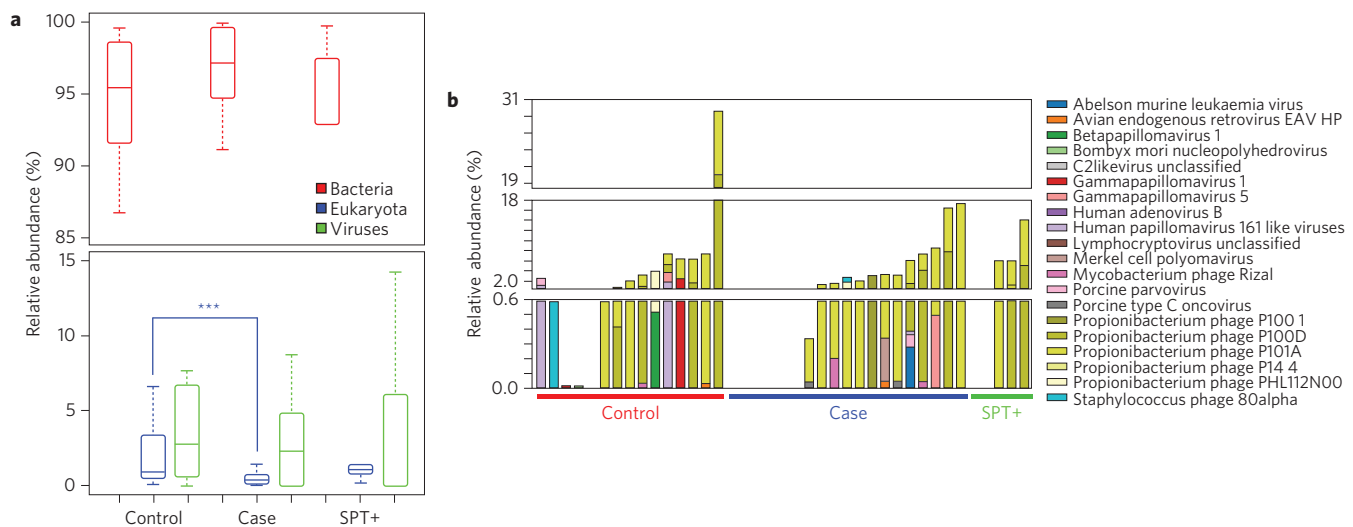
Figure 3 | Eukaryotic and viral diversity in AD-associated skin microbiomes. a, Box plot depicting the relative abundance of bacteria, eukaryotes and viruses in the skin microbiomes (Ac) of normal controls (n = 15), AD cases (n = 19) and SPT+ volunteers (n = 5). **b**, Bar chart depicting the relative abundance of different viruses and phages present in the skin microbiomes of volunteers in the cohort (stratified by groups). All *P* values were calculated using the two-sided Wilcoxon rank-sum test. ***P < 0.01. SPT+ refers to skin prick test positive non-AD volunteers. Box plot whiskers represent 1.5 × interquartile range or the maximum/minimum data point within the range.

Figs 3a and 4b). The next most common eukaryotic member, the *Aspergillaceae* family, was not depleted on AD skin (Fig. 4a). Several species in the *Malassezia* genus have been implicated in skin pathologies including AD[36,37], although these associations lack consensus[37]. Here, reference genomes for all 14 species in the genus[38] were used to quantitate patterns of *Malassezia* colonization in AD and normal individuals. Our data confirmed the predominance of *M. globosa* and *M. restricta* on human skin (Fig. 4c). Additionally, we observed a higher relative abundance of *M. globosa* in controls relative to AD group (*P* < 0.05, Wilcoxon rank-sum test; Fig. 4d), in agreement with its preference for lipid-rich environments. In contrast, *M. dermatis* (*P* < 0.1, Wilcoxon rank-sum test) and *M. sympodialis* were observed to be at higher relative abundance in the AD group (Fig. 4d). Our data provide evidence supporting the previously reported role of *M. sympodialis* in AD[39] and, in addition, associate *M. dermatis* with AD skin.

Alterations in the functional potential of AD-associated microbiome suggest a mechanism for escalation to flare. Differences in the AD skin microbiome may be due to the inability of a subset of homeostatic commensals to thrive in the lipid-depleted habitat of barrier-defective skin, creating ecological space for colonization by pathogens. Microbial shifts in turn could modulate the skin microenvironment to affect AD progression. For instance, elevated skin pH during flares and surface lipid deficiency in AD have been observed previously[40]. We analysed the skin microbiome gene repertoire for functional capabilities in the control group versus the AD group. We observed significant differences with the AD samples, showing lower-than-control levels of potentially beneficial functions contributing to greater skin moisture (for example, the steroid biosynthesis pathway) and reduced skin inflammation (for example, tryptophan metabolism, a modulator of immune response[41]), as well as reduced eukaryotic cellular pathways as expected from the lower eukaryotic relative abundance (Fig. 5a). In contrast, the AD group was enriched in pathogenesis-associated pathways such as bacterial secretion systems[42] and DNA recombination and repair[43].

Intriguingly, AD samples exhibited enrichment in nitrogen, arginine and proline metabolism pathways, which are associated with

ammonia production (Fig. 5a). Elevated skin pH during AD flares accelerates desquamation, increases epidermal barrier permeability and reduces anti-microbial acid stress[40]. Our data confirm higher metagenomic abundance of all three enzymes responsible for metabolizing arginine and citrulline into ammonia in the AD-associated microbiome (Fig. 5b,c), establishing its capacity to promote a less favourable (high pH) microenvironment for skin health. Combined with earlier work showing that arginine and citrulline catabolism is exploited by skin pathogens in combating acid stress[44], this provides a mechanism for enhanced microbial virulence in AD through increased ammonia production.

Discussion
The involvement of the skin microbiome in various diseases has been of significant recent interest[20,45], although its role in AD has only been analysed under flare conditions or using marker genes[19,46]. This study was based on the hypothesis that deeper levels of detail can be determined by whole-metagenome analysis of microbial variations during non-flare periods.

Whole-metagenome sequencing offers the opportunity for multi-kingdom analysis and functional insights into diseases. Metagenomic skin studies have been limited due to the complexity of sampling efficiently[21,47], with no known studies in a disease context. The results presented here demonstrate that whole-metagenome profiling of skin with tape-stripping can be achieved in a clinically practical and robust fashion, while being minimally invasive[47] and avoiding skin-surface disruption with a surgical blade[21]. Our benchmarks demonstrate that the results obtained are consistent with alternative sampling approaches, serving as a useful guide for future studies.

We observed distinct differences between baseline skin microbiomes of AD flare-prone subjects and normal healthy individuals. Strikingly, we did not observe the marked overall dysbiosis or diversity reduction that has been reported during flares[19]. As more microbial diversity is retained in the asymptomatic cohort, their inter-flare microbiome has provided additional insights. For example, the potential pathobionts identified here, including *Streptococcus*, *Gemella* and *Haemophilus* species, have been reported to be enriched in children compared to adults[48], which concurs with the higher incidence of AD in children.
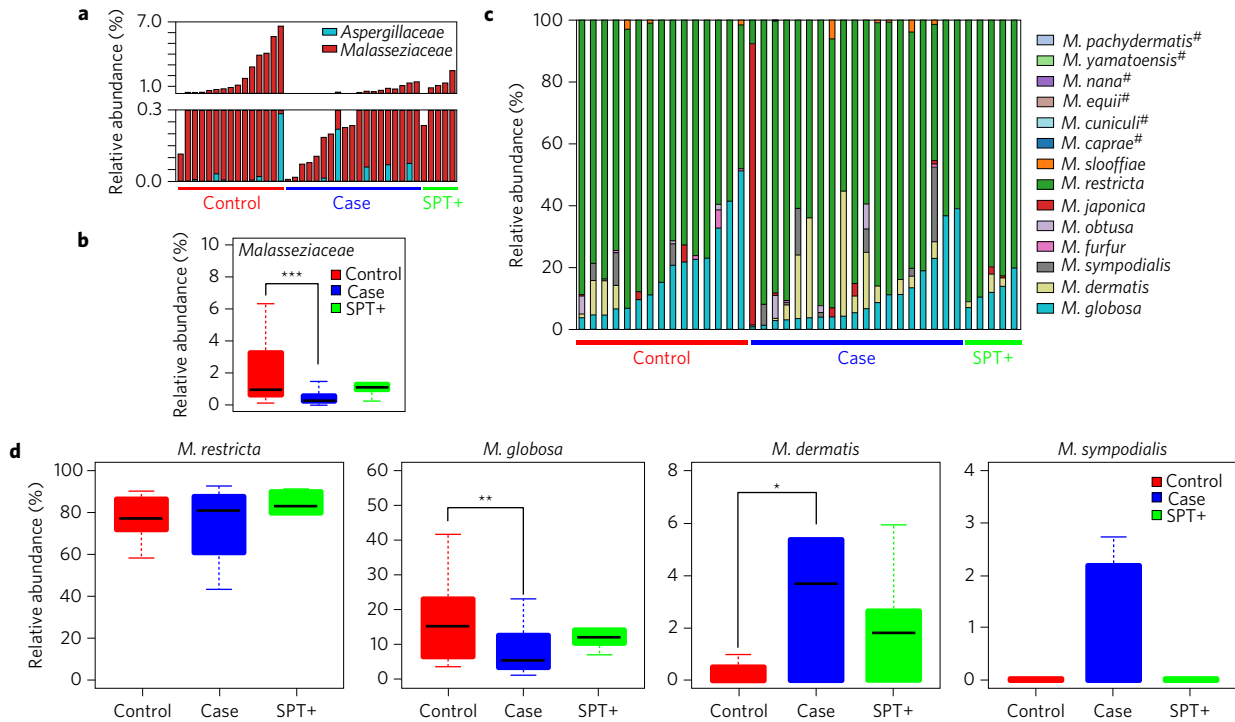
Figure 4 | Changes in *Malassezia* species composition associated with AD. a, Bar chart depicting the relative abundance of different eukaryotes present in the skin microbiomes of volunteers in the cohort (stratified by groups). **b**, Box plot showing the relative abundances of *Malasseziaceae* in the skin microbiomes of normal controls ($n = 15$), AD cases ($n = 19$) and SPT+ volunteers ($n = 5$). **c**, Bar chart depicting the relative abundance of 14 different *Malassezia* species in the skin microbiomes of normal controls ($n = 15$), AD cases ($n = 19$) and SPT+ volunteers ($n = 5$). #Absent in all volunteers. **d**, Box plots showing the relative abundance of selected *Malassezia* species (*M. restricta*, *M. globosa*, *M. dermatis* and *M. sympodialis*) in the skin microbiomes of volunteers in the cohort (stratified by groups). SPT+ refers to skin prick test positive non-AD volunteers. All *P* values were calculated using the two-sided Wilcoxon rank-sum test. ***$P < 0.01$, **$P < 0.05$, *$P < 0.1$. Box plot whiskers represent 1.5 × interquartile range or the maximum/minimum data point within the range. Where black bars are not shown the median is exactly 0.

Our results provide evidence that AD-associated microbiomes can elevate the risk of flares by influencing the skin surface microenvironment and through interaction with the host immune system, although additional work is needed to understand strain-specific differences. Overall, while *Staphylococci* enriched during flares invoked the strongest *in vitro* cytokine and chemokine response, bacterial genera depleted in inter-flare skin elicited a muted response. However, none of the species invoked a strong anti-inflammatory response, suggesting any protective role from depleted commensals may be mediated through alternative mechanisms, such as the ability to crowd out pathogens. These assays have limitations, being *in vitro*, using cells from normal individuals and bacterial isolates not from individuals in our cohort. Additionally, strain variation can significantly impact phenotypes[49]. Nevertheless, the challenge and inhibition assays in this study serve as a preliminary indication that AD-associated bacteria have different functional roles. Understanding the inter-relationships between various species/strains and their contribution in priming the host will further guide the development of rational interventions to restore microbial balance, improve skin health and avoid AD flares.

The fungal component of the microbiome plays an important role in defining the skin microenvironment. *Malassezia* is typically dominant on human skin, and its presence has often been associated with AD[37]. Whole-metagenome data allowed us to characterize, for the first time, a decreased *Malassezia* relative abundance in AD-associated microbiomes. Reduced surface lipids and/or the presence of higher anti-*Malasseziaceae* IgE levels in AD could restrict *Malassezia* ecological competitiveness[50]. Additionally, our analysis revealed an enrichment of *Malassezia* species (*M. dermatis*, *M. sympodialis*) in AD-susceptible skin, suggesting the biological relevance of species switching in AD pathology.

The observed depletion of specific bacterial genera in baseline AD-associated microbiota (and not in SPT+ individuals) indicates that they may have a protective role against AD. This could be through immune quiescence (as observed for *D. nishinomiyaensis*), the production of metabolites and proteins with anti-inflammatory/antimicrobial properties (for example, by metabolically versatile *Deinococci* with anti-oxidant properties on skin; http://www.deinove.com), or by nutritionally out-competing pathogenic species in healthy skin. As specific *Dermacocci* and *Deinococci* are commonly present on healthy human skin, they have the potential for safe application as probiotics for AD, opening up additional therapeutic strategies for exploration.

In addition to modulating the immune system, we show that the AD-associated skin microbiome is primed to generate excess ammonia. This provides a microbial explanation for the higher skin pH associated with AD flares, which in turn could favour a pathogenic skin microbiome[40]. From a therapeutic perspective, correcting metabolite imbalances is an attractive option; ammonia-oxidizing bacteria have been proposed to be a component of healthy human skin, eradicated by the use of modern soaps (http://www.aobiome.com), and we did not detect any ammonia-oxidizing bacteria (for example, *Nitrosomonas*) in this study. The possibility that the depletion of ammonia-oxidizing bacteria increases the risk of AD provides an alternative explanation for the association between increased hygiene and global increase in AD.

This study was initiated to test the hypothesis that microbiome changes offer a 'canary in the coal mine' solution to predicting disease outcomes. The results obtained strongly validate this hypothesis, providing evidence that the AD-colonizing microbiome is likely to impact the skin microenvironment and promote a pro-
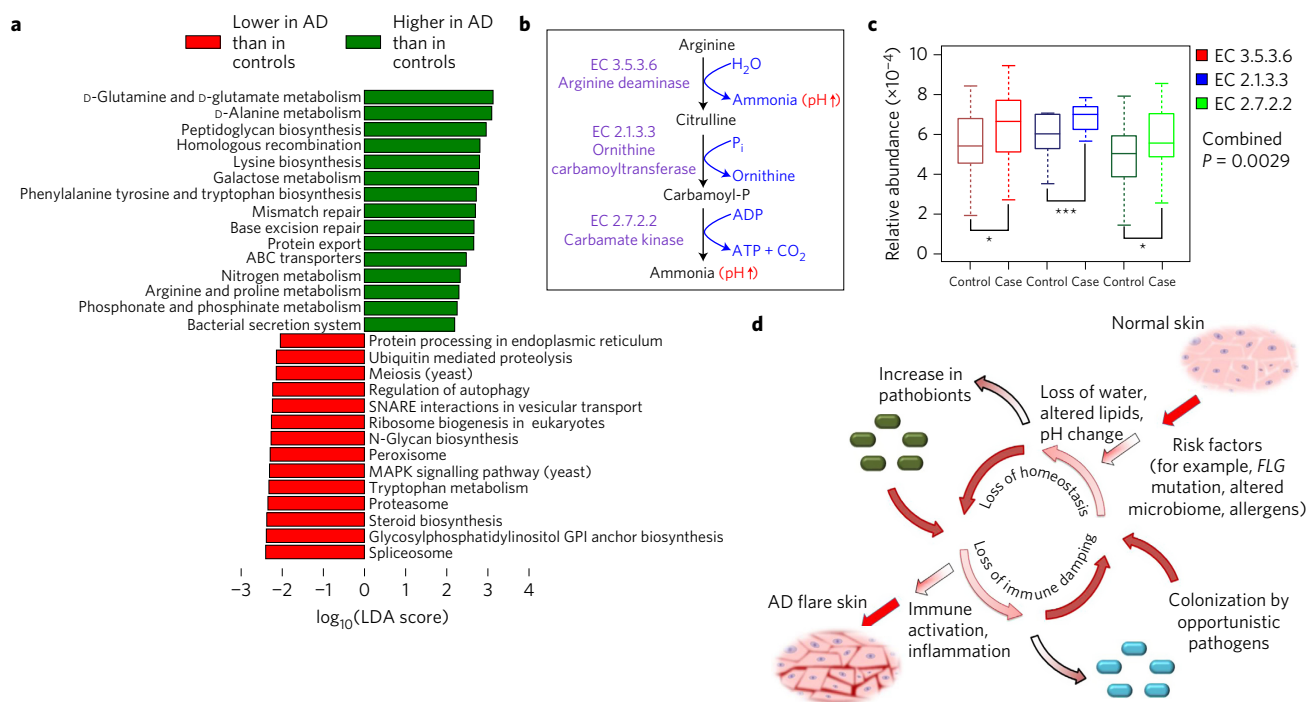
Figure 5 | Functional and metabolic shifts in the AD skin microbiome. a, Pathways that were found to be differentially abundant between the skin microbiomes of normal and non-flare AD individuals. **b**, Reaction steps for the metabolic conversion of arginine to ammonia. **c**, Box plots showing the relative abundance of core enzymes (EC, Enzyme Commission identifier number) for converting arginine to ammonia in the skin microbiomes of normal controls and AD cases. All P values were calculated using one-sided student's t-test and combined using Fisher's combined probability test (***$P < 0.01$, **$P < 0.05$, *$P < 0.1$). **d**, A model for microbiome-dependent progression from normal skin to AD flare skin involving a feedback loop between skin microbiota, skin microenvironment and host immune response. Box plot whiskers represent 1.5 × interquartile range or the maximum/minimum data point within the range.

inflammatory phenotype (Fig. 5d). The altered microenvironment and loss of homeostatic microbiota leave the epidermis vulnerable to transitions from opportunistic to pathogenic microbial colonization (Fig. 5d). Although it is hard to calculate the quantal effect of dysbiosis on population prevalence and severity, it is clear that microbiome interactions provide additional complexity to AD pathogenesis. With the ever increasing sensitivity of genomic techniques, we predict that observing microbial changes will increasingly become a feasible, non-invasive and cheap method to monitor skin health and aid probiotic treatment strategies.

Methods

Cohort recruitment and stratification. Volunteers for the study were from an established cohort[22], recruited using a cross-sectional sampling approach from the National University of Singapore (NUS) campus. All participants were above the age of 18 years. Recruitment was approved by the Institutional Review Board (NUS IRB reference code 07-023 and NUS 10-343) and was in accordance with the Helsinki Declaration. Informed consent was obtained from all subjects recruited into the study. Cohort stratification was performed with epidemiological data collected for clinical history of atopic diseases (according to the ISAAC protocol[25]) and skin prick reactions to known allergens as detailed in the following[22].

Participants were tested for their atopic status by performing a skin prick test (SPT). Specifically, participants were tested for four aeroallergens, *Dermatophagoides pteronyssinus*, *Blomia tropicalis*, *Elaeis guineensis* and *Curvularia lunata*. Validation of SPT was performed with positive (histamine) and negative (saline) controls. SPT was considered positive when the weal diameter was ≥3 mm, whereas no sign of weal and erythema was considered a negative SPT. Participants with a <3 mm reaction for histamine, or an erythema/weal to saline, or with a <3 mm reaction to the test allergens were excluded from analysis. The skin-prick reactivities to dust mites (especially the two species *B. tropicalis* and *D. pteronyssinus*) are highly sensitive and specific markers for allergic sensitization in Singapore[51]. Thus, together with the positive and negative controls, a positive reaction to either of the dust mites indicated positive SPT, a marker of atopy.

Sample collection. Three different collection methods for skin microbiome sampling were tested: tape stripping, swab sampling and the cup scrub method.

Tape stripping. Adhesive tape discs (D-Square Standard Sampling Discs; Cuderm) still attached to the plastic backing (to protect the sticking surface) were completely soaked in 70% ethanol for 1 min and wiped dry with paper towels before placement on the antecubital fossa (Ac) or the retroauricular crease (Ra) of subjects. Pressure was applied on the tape disc with a D-Square Pressure Instrument (Cuderm) before peeling off. This cycle of sticking and peeling was repeated approximately 50 times with the same tape disc over a period of 2 min on a delimited area (3 cm²) of skin regions Ac or Ra to saturate the adhesive tape disc with skin surface material to maximize DNA collection. We also tested applying pressure without the D-Square Pressure Instrument (using the thumb instead), and no difference was observed in the total amount of DNA collected. Similar approaches were originally used for proteomic and metabolomic studies[52,53].

Swab sampling. In the swab collection method, a sterile swab (Catch-All Sample Collection Swab; Epicentre) was soaked in phosphate buffer saline (PBS) + 0.1% vol/vol Triton-X100 and was applied immediately to skin regions Ac or Ra, not overlapping with the area where tape strip samples were collected. The swab was rubbed for 1 min to collect biological material from the skin surface. This approach potentially has the drawback of low DNA yield.

Cup scrub method. A hollow cylinder (internal diameter 25 mm) was soaked in 70% ethanol for 1 min, wiped with tissue and allowed to dry completely before placement onto a non-overlapping sampling region of the Ac. A volume of 1 ml PBS + 0.1% vol/vol Triton-X100 was added into the hollow cylinder. The entire surface of the skin within the hollow cylinder was rubbed with an inoculating loop for 1 min and the liquid was then transferred into a 1.5 ml tube. Similar approaches have been widely used for culture-based studies[54,55] but can be cumbersome to use in a clinical setting. All samples were stored at −20 °C before further processing.

After the initial experiments comparing tape, swab and cup scrub sampling approaches, all samples from the epidemiologically stratified cohort were collected with adhesive tape discs adjacent to the Ac region, as described above. Participants were allowed to maintain a healthy skin care regimen, and only restricted for antibiotics, based on prior observations that discontinuing medications and emollients for AD patients frequently leads to dysbiosis similar to what is seen in AD flares[19].

DNA extraction. Tape discs and swabs were transferred into Lysing Matrix E tubes (MP Biomedicals) and 600 µl of ATL buffer (Qiagen) was added. Samples collected using the cup scrub method were first subjected to centrifugation at 9,300g for 3 min. Cell pellets were subsequently re-suspended with 600 µl of ATL buffer (Qiagen). All samples were subjected to bead-beating with a FastPrep-24 Instrument (MP Biomedicals) at a speed of 6.0 m s⁻¹ for 40 s. Samples were centrifuged at 16,000g for

5 min and the supernatant was treated with Proteinase K (Qiagen) and incubated at 56 °C for 15 min. DNA was extracted using an EZ1 Advanced XL Instrument (Qiagen) with the EZ1 DNA Tissue Kit (Qiagen) and was quantified using the Qubit dsDNA HS Assay Kit (Life Technologies) and later stored at −20 °C.

16S PCR. PCR was carried out using primers 338F (5′-ACTCCTACGGGAGGCWG C-3′) and 1061R (5′-CRRCACGAGCTGACGAC-3′) and the HotStar HiFidelity Polymerase Kit (Qiagen) according to the manufacturer's manual with the exception of primer concentrations (0.5 μM), and the addition of $MgSO_4$ at a final concentration of 2 mM. The conditions for PCR were as follows: initial denaturation at 95 °C for 5 min, 35 cycles of denaturation at 95 °C for 30 s, annealing at 59 °C for 30 s, and extension at 72 °C for 1 min, followed by a final extension at 72 °C for 6 min. PCR products were purified with Agencourt AMPure XP (Beckman Coulter), and amplicons were visualized using an Agilent Bioanalyzer, prepared with an Agilent DNA1000 Kit (Agilent Technologies).

Library construction. Adaptive Focused Acoustics (Covaris) was used to shear a standard volume of 50 μl of the extracted DNA. DNA libraries were prepared using GeneRead DNA Library I Core Kit (Qiagen) according to the manufacturer's protocol with the use of barcode adapters in place of the GeneRead Adapter I Set. Custom index-primers were used for enrichment of the DNA libraries, which was performed according to an enrichment protocol adapted from the Multiplexing Sample Preparation Oligonucleotide kit (Illumina). Libraries were quantified using an Agilent Bioanalyzer, prepared with the Agilent High Sensitivity DNA Kit (Agilent Technologies). Of the 80 libraries built for profiling normal controls, the AD group and SPT+ volunteers, one library was unsuccessful. Thus, its accompanying pair was omitted from further analysis. Paired-end sequencing (2×101 bp reads) was performed on successful DNA libraries using an Illumina HiSeq 2000 instrument at the Genome Institute of Singapore to generate around 589 million paired-end reads in total and 7.55 million paired-end reads on average per library.

Read preprocessing. Sequencing bases with quality scores lower than 3 were trimmed off the 3′ ends of reads. Read pairs with a read shorter than 60 bp were discarded. For the 16S sequencing data sets, reads from the target region were identified by mapping (using BWA-MEM with default parameters) to the 16S database provided with the program EMIRGE[56]. For the whole metagenome sequencing data sets, human reads were filtered out by mapping to the human genome (hg19) using BWA-MEM[57] with default parameters (version 0.7.9a). Overall, around 27.4% of the reads were found to be usable after filtering for human contamination.

Community profiling, differential abundance and correlation analysis.
16S profiling with filtered 16S reads was performed as described previously[58]. In brief, EMIRGE[56], a probabilistic expectation-maximization-based algorithm, was used to de novo reconstruct and measure the abundances of 16S rRNA sequences (with default parameters). The reconstructed sequences were then taxonomically classified using BLAST against the NR database. For whole metagenome shotgun profiling, MetaPhlAn[59] or MetaPhlAn v2.0 (default parameters) was used to determine bacterial, viral and eukaryotic community abundances. Pearson correlation matrices between different sampling and profiling strategies were plotted using the R package 'corrplot'. Differentially abundant taxa between cases and controls were conservatively identified using the non-parametric Wilcoxon rank-sum test (two-sided) and P values were corrected using p.adjust in R using the false discovery rate option. Bacterial genera with mean abundance of less than 0.1% (as determined by MetaPhlAn) across AD cases and normal controls were excluded for this analysis. Box plots were drawn with the parameter 'outpch = NA' (outliers not shown) using R. Principle coordinates analysis of the genus composition was performed based on Bray–Curtis dissimilarity using the R package 'phyloseq'. Correlations between bacterial taxa were used to identify potential bacterial interactions in skin flora. For this analysis, taxa with a mean abundance (across all samples) below 0.1% were excluded and taxa pairs with a Spearman correlation coefficient (ρ) greater than 0.3 (absolute value) and FDR adjusted $P < 0.05$ were reported (Supplementary Table 6).

Bacteria strain variation analysis. To identify the *S. aureus* and *S. epidermidis* strains present, reference genomes were downloaded from NCBI (ftp://ftp.ncbi.nlm.nih.gov/genomes/archive/old_refseq/; 39 complete genomes for *S. aureus*, 2 complete and 61 draft genomes for *S. epidermidis*). Microbiome reads from all samples were pooled and mapped to the genomes of *S. aureus* using Pathoscope2 (default parameters) with the genomes of *S. epidermidis* as decoys (to identify *S. aureus* strains) and vice versa (to identify *S. epidermidis* strains). Potential false positives were filtered out based on <10% of the strain genome (in 10 kbp non-overlapping bins) having read coverage[38]. Strain genomes with less than 1% of total mapped reads were also excluded before remapping the microbiome reads from each individual to selected genomes to quantify strain abundances. The reference strains selected for *S. aureus* were CN1 (uid217769; strain-5), JH1 (uid58457; strain-4), MSHR1132 (uid89393; strain-3), MSSA476 (uid57841; strain-2), ST398 (uid159247; strain-1), and for *S. epidermidis* were A487 (uid199704; strain-6), M23864_W1 (uid55897 strain-5), NIHLM023 (uid180512; strain-4), NIHLM039 (uid180510; strain-3), SK135 (uid42967; strain-2) and VCU129 (uid180073; strain-1).

Differential SNP analysis of staphylococcal virulence genes. Virulence factors of *S. aureus* MW2 were downloaded from the virulence factors database[60] (http://www.mgc.ac.cn/VFs/). Microbiome reads from cases and controls were mapped against virulence gene sequences using BWA-MEM[57] (version 0.7.9a) with default parameters. For each sample, we created a per-base pileup profile using the plpsummary module in LoFreq (version 2.1.1) (with '–use-orphan' option to include orphan reads)[61]. For each position, we only considered the two most frequent alleles across all the samples, and we tested the difference in allele frequencies between the two groups (case and control) using the non-parametric Wilcoxon rank-sum test (two-sided).

Agar diffusion assays. The bacterial species studied here (*Staphylococcus aureus* 31240, *Staphylococcus epidermidis* 12228, *Streptococcus cristatus* 51100, *Streptococcus mitis* 49456, *Streptococcus pyogenes* 49117, *Streptococcus salivarius* 7073 and *Streptococcus sanguinis* 49295) were obtained from ATCC. Bacteria were cultured in BHI broth (Supplementary Table 9) at 37 °C overnight and the optical density at 600 nm (OD_{600nm}) was measured for each culture. Each culture was diluted to an OD_{600nm} of 0.1 with fresh media (with the exception of *S. sanguinis*, which was diluted to $OD_{600nm} = 0.4$) in a total of 4 ml BHI broth and incubated at 37 °C with agitation. Bacterial cultures were allowed to grow to an OD that corresponds to the log-phase of the bacteria (that is, *S. epidermidis*, OD = 1.9; *S. mitis*, OD = 1.7; *S. salivarius*, OD = 2.3; *S. pyogenes*, OD = 1.5; *S. cristatus*, OD = 1.8; *S. sanguinis*, OD = 2.1). The *S. aureus* bacterial lawn was made by diluting the culture to a final concentration of 10^6 c.f.u. ml^{-1} in 8 ml 0.7% BHI agar and gently mixing the agar by rotating it in a 50 ml falcon tube. The bacteria/agar mixture was poured over a BHI agar plate and left to solidify. Filter paper discs (Whatman filter paper no. 1, 1.5 cm) were then submerged in other bacterial cultures until they were saturated, and then gently layered over the solidified bacterial lawn. The agar plate was incubated at 37 °C and checked for clearing zones the following day.

Bacterial cultures for keratinocyte and moDC challenge assays. We cultured six bacteria (identities confirmed by Sanger sequencing of the 16S rRNA gene): *Dermacoccus profundi* BAA-2375, *Dermacoccus nishinomiyaensis* 29093, *Deinococcus radiodurans* 13939, *Staphylococcus aureus* subsp. aureus 31240, *Staphylococcus epidermidis* 12228 and a *Bacillus firmus* isolate. The bacteria were grown under culture conditions as summarized in Supplementary Table 8 for either 24 or 48 h. The bacteria were grown overnight or over two nights and we then measured the OD_{600nm}. The ODs were calculated and brought to $OD_{600nm} = 1$ and were further diluted to 0.01 with fresh media. The OD was measured at 1 or 3 h intervals, depending on whether the bacterial growth conditions were 24 or 48 h, respectively. In parallel, bacterial cultures were also plated on agar of their corresponding growth medium at a dilution of 10^{-3} to 10^{-7} in replicates of four, for each time point. Agar plates were incubated overnight or over two nights. The colony-forming units per millilitre (c.f.u. ml^{-1}) were then calculated and the growth curves were plotted. We next observed the mid-log phase of bacterial growth. This was the OD we selected at which to collect the bacteria for subsequent bacterial agonist immunological assays. Three conditions were collected at mid-log phase: bacterial media alone, bacterial culture and supernatant of bacterial culture. Optical densities were taken once again for comparison to the original growth curves to verify that the growth kinetics had not changed between the bacterial growth experiments. Bacteria collected at the mid-log phase were normalized to the lowest c.f.u. ml^{-1} bacterial count so that equal amounts of c.f.u. were added to the subsequent bacterial agonist immunological assays.

Keratinocyte cell culture and profiling. Normal human epidermal keratinocytes (NHEKs) immortalized with the telomerase catalytic subunit, named N/TERT-1[62] were cultured in K-SFM (Life Technologies) supplemented with 0.2 ng ml^{-1} epidermal growth factor (EGF), 25 μg ml^{-1} bovine pituitary extract (BPE), 0.4 mM $CaCl_2$ and penicillin/streptomycin (1×). The cells were tested to be negative for mycoplasma contamination using the MycoAlert PLUS mycoplasma detection kit (Lonza) according to the manufacturer's instructions. For bacterial challenge assays, N/TERT-1 cells were grown to 80% confluence in 10 cm dishes by switching the culture medium to an equal ratio mixture of K-SFM medium and DF-K medium, which is Ham's F-12 and Ca^{2+}- and glutamine-free DMEM (1:3) supplemented with 0.2 ng ml^{-1} EGF, 25 μg ml^{-1} BPE, 1.5 mM glutamine without the addition of antibiotics. After 24 or 48 h, supernatants were collected from the wells for cytokine profiling.

Dendritic cell culture and profiling. moDCs were generated as reported previously[63]. Briefly, peripheral blood mononuclear cells from healthy donors (Institutional Review Board approval NUS-IRB 10-250) were isolated by density centrifugation (Ficoll-Paque; GE Healthcare) and monocytes were isolated by positive selection of CD14+ cells with CD14 microbeads (Miltenyi Biotec). Monocytes were cultured in antibiotic-free medium (RPMI 1640 with 10% FBS, 1 mM pyruvate, 2 mM L-glutamine, 50 mM 2-ME, non-essential amino acids and 15 mM HEPES) and supplemented with GM-CSF and IL-4 (both 1,000 U ml^{-1}, Miltenyi Biotec). At days 4 and 6, fresh cytokines were added into the culture. Cells were either treated with different concentrations of bacteria, supernatant or bacterial culture medium at day 6 or left untreated. At day 8, immature (untreated), bacterial/supernatant/medium-treated moDCs were collected and washed for further experiments.

Cytokine analysis for keratinocytes and moDCs. For cytokine profiling, supernatants from keratinocyte and moDC culture wells were collected and then used for multiplex analysis by a human cytokine/chemokine bead panel 1 (MilliplexMap, Millipore) and Flexmap 3D system (Luminex). The levels of 30 protein content (epidermal growth factor (EGF), eotaxin, fibroblast growth factor 2 (FGF-2), Fms-like tyrosine kinase 3 (Flt-3), fractalkine, granulocyte colony-stimulating factor (G-CSF), growth-regulated oncogene (GRO), interferon-alpha 2 (IFNa2), interleukin-10 (IL-10), IL-12p40, IL-12p70, IL-1Ra, IL-1a, IL-1b, IL-6, IL-8, interferon gamma-induced protein 10 (IP-10), macrophage inflammatory protein-1 (MCP-1), MCP-3, macrophage-derived chemokine (MDC), macrophage inflammatory protein-1 (MIP-1α), MIP-1β, platelet derived growth factor-AB/BB (PDGF-AA), PDGF-AB/BB, regulated upon activation, normal T cell expressed and secreted (RANTES), transforming growth factor-α (TGF-α), TNF-α, TNF-β, vascular endothelial growth factor (VEGF), soluble CD40 ligand (sCD40L)) were measured from the cell culture supernatants.

Preparation and isolation of epidermal LCs. Human skin samples were obtained with approval and in accordance with the Singapore National Healthcare Group Research Ethics Committee. Epidermal cell suspensions were prepared as described previously[64]. Briefly, strips of 200 μm whole skin sections were incubated with 2 U ml⁻¹ dispase (ThermoFisher Scientific) in RPMI 1640 at 37 °C for 1 h to separate the epidermis from dermis. Epidermal sheets were further digested with 0.80 mg ml⁻¹ collagenase (Type IV, Worthington-Biochemical) in RPMI 1640 with 10% FCS and 0.05 mg ml⁻¹ DNase (Sigma-Aldrich) at 37 °C overnight. Epidermal LCs (CD1a^hi Langerin^hi) were isolated by fluorescence activated cell sorting (FACS) with a FACSAriaII (BD Biosciences).

Epidermal LCs from mice were isolated as described previously[65]. Sex (male) and age (7–8 weeks) matched C57BL/6 were used. Approval was obtained from the Institutional Animal Care and Use Committee, Biological Resource Center, A*STAR, Singapore. Briefly, mouse ears were split into dorsal and ventral halves and floated in 4 U ml⁻¹ dispase in RPMI 1640 at 37 °C for 1 h to allow separation of the epidermal and dermal sheets. Epidermal sheets were cut into small pieces and incubated in 0.1 mg ml⁻¹ collagenase type IV (Sigma-Aldrich) at 37 °C for 1 h. Cells were passed through a 19 G syringe and filtered through a 70 μM nylon mesh to obtain a homogeneous cell suspension. LCs (CD24^hi EpCAM^hi) were isolated by FACS.

Flow cytometry. The following anti-human antibodies were used: V500-conjugated CD45 (clone HI30, BD Biosciences), PerCp/Cy5.5-conjugated HLA-DR (clone LN3, eBioscience), APC/Cy7-conjugated CD14 (clone HCD14, BioLegend), Alexa Fluor 700-conjugated CD1a (clone HI149, BioLegend) and PE-conjugated Langerin (clone DCGM4, Beckman Coulter). The following anti-mouse antibodies were used: FITC-conjugated CD45 (clone 30-F11, BioLegend), Alexa Fluor 700-conjugated MHC II (clone M5/114.15.2, eBioscience), PE-conjugated CD103 (clone 2E7, eBioscience), PerCp/Cy5.5-conjugated CD11b (clone M1/70, eBioscience), PE/Cy7-conjugated Ep-CAM/CD326 (clone G8.8, BioLegend), eFluor 450-conjugated CD24 (clone M1/69, eBioscience).

Bacterial cultures for human and mouse LC challenge assays. Four bacteria, *D. nishinomiyaensis* 29093, *D. radiodurans* 13939, *S. aureus* 31240 and *S. epidermidis* 12228, were grown overnight in BHI media at 37 °C. OD_{600nm} was measured for overnight cultures, and fresh cultures were prepared for each bacteria, starting from an OD of 0.01. Bacterial cultures were grown to the following ODs: *S. aureus*, OD = 1.9; *S. epidermidis*, OD = 2; *D. radiodurans*, OD = 2; *D. nishinomiyaensis*, OD = 3. Cultures were centrifuged at 8,000g for 15 min to sediment the cells. Supernatant was filtered with a 0.22 μm syringe filter, and 100 μl supernatant was plated onto BHI agar plates to check for the presence of bacterial cells. Heat inactivation of bacteria was performed by placing cultures in a 70 °C water bath for 3 h, and heat inactivation was confirmed by the absence of detectable bacteria on BHI agar plates for up to 3 days. Cells were seeded in 96-well V-bottom plates (Costar, Corning) for the bacterial challenge assays. Sterile filtered bacterial supernatants were added to the wells at a final dilution of 100× and incubated for 24 h at 37 °C. For bacterial co-culture, LCs were challenged with bacteria at a multiplicity of infection (MOI) of 0.1 for 24 h. After incubation, cell supernatants were collected for cytokine analysis. Negative control cultures contained cells co-incubated with BHI medium.

Cytokine analysis for human and mouse LCs. Cytokine production was measured by immunoassay with the human or mouse cytokine/chemokine bead panel (MilliplexMap, Millipore) and Flexmap 3D system (Luminex). For human samples, EGF, eotaxin, FGF-2, Flt-3L, fractalkine, G-CSF, GM-CSF, GRO, IFNα2, IFNγ, IL-10, IL-12p40, IL-12p70, IL-13, IL-15, IL-17A, IL-1RA, IL-1α, IL-1β, IL-2, IL-3, IL-4, IL-5, IL-6, IL-7, IL-8, IL-9, IP-10, MCP-1, MCP-3, MDC, MIP-1α, MIP-1β, PDGF-AA, PDGF-AB, RANTES, TGF-α, TNF-α, TNF-β, VEGF and sCD40L were analysed. For mouse samples, eotaxin, G-CSF, GM-CSF, IFNγ, IL-10, IL-12p40, IL-12p70, IL-13, IL-15, IL-17, IL-1α, IL-1β, IL-2, IL-3, IL-4, IL-5, IL-6, IL-7, IL-9, IP-10, KC, LIF, LIX, M-CSF, MCP-1, MIG, MIP-1α, MIP-1β, MIP-2, RANTES and TNF-α were analysed.

Abundance profiling of *Malassezia* species. PathoScope 2.0 (ref. 66) was used to quantify the relative abundance of all 14 known *Malassezia* species by mapping microbiome reads to the *Malassezia* reference genomes (target) and a set of other fungal genomes that served as decoys (control; Supplementary Table 10). The approach used in PathoScope first determines reads that have better or unique alignments to the target genomes (compared to the control references) and then uses an expectation-maximization algorithm to reassign reads to the most plausible reference sources and estimate their relative abundances. To further eliminate false positives, we binned the genomes into 1 kb bins and only kept species assignments where more than 10% of the bins were covered by at least one read. Species abundances were then renormalized after this filter.

Pathway analysis. Microbiome reads from cases and controls were mapped to KEGG orthologs using Bowtie2 (ref. 67; version 2.2.4; parameter setting: -k 10). Pathway abundances for cases and controls were estimated using HUMAnN[68] (version 0.99) with default parameters. The abundance table computed by HUMAnN was then analysed with the linear discriminant analysis approach in LEfSe[69] (version 1.1.0) to identify differentially abundant pathways.

References

1. Tay, Y. K., Kong, K. H., Khoo, L., Goh, C. L. & Giam, Y. C. The prevalence and descriptive epidemiology of atopic dermatitis in Singapore school children. *Br. J. Dermatol.* **146,** 101–106 (2002).
2. Asher, M. I. *et al.* Worldwide time trends in the prevalence of symptoms of asthma, allergic rhinoconjunctivitis, and eczema in childhood: ISAAC Phases One and Three repeat multicountry cross-sectional surveys. *Lancet* **368,** 733–743 (2006).
3. Garmhausen, D. *et al.* Characterization of different courses of atopic dermatitis in adolescent and adult patients. *Allergy* **68,** 498–506 (2013).
4. Paternoster, L. *et al.* Multi-ancestry genome-wide association study of 21,000 cases and 95,000 controls identifies new risk loci for atopic dermatitis. *Nature Genet.* **47,** 1449–1456 (2015).
5. Palmer, C. N. *et al.* Common loss-of-function variants of the epidermal barrier protein filaggrin are a major predisposing factor for atopic dermatitis. *Nature Genet.* **38,** 441–446 (2006).
6. van den Oord, R. A. & Sheikh, A. Filaggrin gene defects and risk of developing allergic sensitisation and allergic disorders: systematic review and meta-analysis. *Br. Med. J.* **339,** b2433 (2009).
7. Chen, H. *et al.* Wide spectrum of filaggrin-null mutations in atopic dermatitis highlights differences between Singaporean Chinese and European populations. *Br. J. Dermatol.* **165,** 106–114 (2011).
8. Sandilands, A., Sutherland, C., Irvine, A. D. & McLean, W. H. Filaggrin in the frontline: role in skin barrier function and disease. *J. Cell Sci.* **122,** 1285–1294 (2009).
9. Howell, M. D. *et al.* Th2 cytokines act on S100/A11 to downregulate keratinocyte differentiation. *J. Invest. Dermatol.* **128,** 2248–2258 (2008).
10. Morizane, S. *et al.* TH2 cytokines increase kallikrein 7 expression and function in patients with atopic dermatitis. *J. Allergy Clin. Immunol.* **130,** 259–61 e1 (2012).
11. Howell, M. D. *et al.* Cytokine modulation of atopic dermatitis filaggrin skin expression. *J. Allergy Clin. Immunol.* **124,** R7–R12 (2009).
12. Hvid, M. *et al.* Regulation of caspase 14 expression in keratinocytes by inflammatory cytokines—a possible link between reduced skin barrier function and inflammation? *Exp. Dermatol.* **20,** 633–636 (2011).
13. Brown, S. J. *et al.* Filaggrin haploinsufficiency is highly penetrant and is associated with increased severity of eczema: further delineation of the skin phenotype in a prospective epidemiological study of 792 school children. *Br. J. Dermatol.* **161,** 884–889 (2009).
14. Fallon, P. G. *et al.* A homozygous frameshift mutation in the mouse Flg gene facilitates enhanced percutaneous allergen priming. *Nature Genet.* **41,** 602–608 (2009).
15. Elias, P. M., Hatano, Y. & Williams, M. L. Basis for the barrier abnormality in atopic dermatitis: outside–inside–outside pathogenic mechanisms. *J. Allergy Clin. Immunol.* **121,** 1337–1343 (2008).
16. Kabashima, K. New concept of the pathogenesis of atopic dermatitis: interplay among the barrier, allergy, and pruritus as a trinity. *J. Dermatol. Sci.* **70,** 3–11 (2013).
17. Leyden, J. J., Marples, R. R. & Kligman, A. M. *Staphylococcus aureus* in the lesions of atopic dermatitis. *Br. J. Dermatol.* **90,** 525–530 (1974).
18. Huang, J. T., Abrams, M., Tlougan, B., Rademaker, A. & Paller, A. S. Treatment of *Staphylococcus aureus* colonization in atopic dermatitis decreases disease severity. *Pediatrics* **123,** e808–e814 (2009).

19. Kong, H. H. *et al.* Temporal shifts in the skin microbiome associated with disease flares and treatment in children with atopic dermatitis. *Genome Res.* **22,** 850–859 (2012).

20. Oh, J. *et al.* The altered landscape of the human skin microbiome in patients with primary immunodeficiencies. *Genome Res.* **23,** 2103–2114 (2013).

21. Oh, J. *et al.* Biogeography and individuality shape function in the human skin metagenome. *Nature* **514,** 59–64 (2014).

22. Andiappan, A. K. *et al.* Validation of GWAS loci for atopic dermatitis in a Singapore Chinese population. *J. Invest. Dermatol.* **132,** 1505–1507 (2012).

23. Grice, E. A. *et al.* A diversity profile of the human skin microbiota. *Genome Res.* **18,** 1043–1050 (2008).

24. Mathieu, A., Vogel, T. M. & Simonet, P. The future of skin metagenomics. *Res. Microbiol.* **165,** 69–76 (2014).

25. Asher, M. I. *et al.* International study of asthma and allergies in childhood (ISAAC): rationale and methods. *Eur. Respir. J.* **8,** 483–491 (1995).

26. Manivasagan, P., Venkatesan, J., Sivakumar, K. & Kim, S. K. Pharmaceutically active secondary metabolites of marine actinobacteria. *Microbiol. Res.* **169,** 262–278 (2014).

27. Chiller, K., Selkin, B. A. & Murakawa, G. J. Skin microflora and bacterial infections of the skin. *J. Invest. Dermatol. Symp. Proc.* **6,** 170–174 (2001).

28. Wang, Y. *et al.* Staphylococcus epidermidis in the human skin microbiome mediates fermentation to inhibit the growth of *Propionibacterium acnes*: implications of probiotics in acne vulgaris. *Appl. Microbiol. Biotechnol.* **98,** 411–424 (2014).

29. Schloissnig, S. *et al.* Genomic variation landscape of the human gut microbiome. *Nature* **493,** 45–50 (2013).

30. Kapral, F. A., Smith, S. & Lal, D. The esterification of fatty acids by *Staphylococcus aureus* fatty acid modifying enzyme (FAME) and its inhibition by glycerides. *J. Med. Microbiol.* **37,** 235–237 (1992).

31. Lowe, A. M., Beattie, D. T. & Deresiewicz, R. L. Identification of novel staphylococcal virulence genes by *in vivo* expression technology. *Mol. Microbiol.* **27,** 967–976 (1998).

32. Mlckova, P., Cechova, D., Chalupna, P., Novotna, O. & Prokesova, L. Enhanced systemic and mucosal antibody responses to a model protein antigen after intranasal and intratracheal immunisation using *Bacillus firmus* as an adjuvant. *Immunol. Lett.* **77,** 39–45 (2001).

33. Lutz, M. B. *et al.* An advanced culture method for generating large quantities of highly pure dendritic cells from mouse bone marrow. *J. Immunol. Methods* **223,** 77–92 (1999).

34. Mitsui, H. *et al.* Differential expression and function of Toll-like receptors in Langerhans cells: comparison with splenic dendritic cells. *J. Invest. Dermatol.* **122,** 95–102 (2004).

35. Malissen, B., Tamoutounour, S. & Henri, S. The origins and functions of dendritic cells and macrophages in the skin. *Nature Rev. Immunol.* **14,** 417–428 (2014).

36. Lubbe, J. Secondary infections in patients with atopic dermatitis. *Am. J. Clin. Dermatol.* **4,** 641–654 (2003).

37. Darabi, K., Hostetler, S. G., Bechtel, M. A. & Zirwas, M. The role of Malassezia in atopic dermatitis affecting the head and neck of adults. *J. Am. Acad. Dermatol.* **60,** 125–136 (2009).

38. Wu, G. *et al.* Genus-wide comparative genomics of malassezia delineates its phylogeny, physiology, and niche adaptation on human skin. *PLoS Genet.* **11,** e1005614 (2015).

39. Casagrande, B. F. *et al.* Sensitization to the yeast *Malassezia sympodialis* is specific for extrinsic and intrinsic atopic eczema. *J. Invest. Dermatol.* **126,** 2414–2421 (2006).

40. Cork, M. J. *et al.* Epidermal barrier dysfunction in atopic dermatitis. *J. Invest. Dermatol.* **129,** 1892–1908 (2009).

41. Moffett, J. R. & Namboodiri, M. A. Tryptophan and the immune response. *Immunol. Cell Biol.* **81,** 247–265 (2003).

42. Lee, V. T. & Schneewind, O. Protein secretion and the pathogenesis of bacterial infections. *Genes Dev.* **15,** 1725–1752 (2001).

43. Zgur-Bertok, D. DNA damage repair and bacterial pathogens. *PLoS Pathogens* **9,** e1003711 (2013).

44. Cusumano, Z. T., Watson, M. E.Jr & Caparon, M. G. *Streptococcus pyogenes* arginine and citrulline catabolism promotes infection and modulates innate immunity. *Infect. Immun.* **82,** 233–242 (2014).

45. Grice, E. A. & Segre, J. A. The skin microbiome. *Nature Rev. Microbiol.* **9,** 244–253 (2011).

46. Dekio, I. *et al.* Characterization of skin microbiota in patients with atopic dermatitis and in normal subjects using 16S rRNA gene-based comprehensive analysis. *J. Med. Microbiol.* **56,** 1675–1683 (2007).

47. Garcia-Garcera, M., Garcia-Etxebarria, K., Coscolla, M., Latorre, A. & Calafell, F. A new method for extracting skin microbes allows metagenomic analysis of whole-deep skin. *PLoS One* **8,** e74914 (2013).

48. Oh, J., Conlan, S., Polley, E. C., Segre, J. A. & Kong, H. H. Shifts in human skin and nares microbiota of healthy children and adults. *Genome Med.* **4,** 77 (2012).

49. Conlan, S. *et al.* Staphylococcus epidermidis pan-genome sequence analysis reveals diversity of skin commensal and hospital infection-associated isolates. *Genome Biol.* **13,** R64 (2012).

50. Zhang, E. *et al.* Anti-malassezia-specific IgE antibodies production in Japanese patients with head and neck atopic dermatitis: relationship between the level of specific IgE antibody and the colonization frequency of cutaneous Malassezia species and clinical severity. *J. Allergy (Cairo)* **2011,** 645670 (2011).

51. Andiappan, A. K. *et al.* Allergic airway diseases in a tropical urban environment are driven by dominant mono-specific sensitization against house dust mites. *Allergy* **69,** 501–509 (2014).

52. Broccardo, C. J., Mahaffey, S. B., Strand, M., Reisdorph, N. A. & Leung, D. Y. Peeling off the layers: skin taping and a novel proteomics approach to study atopic dermatitis. *J. Allergy Clin. Immunol.* **124,** 1113–1115 (2009).

53. Kezic, S., Kammeyer, A., Calkoen, F., Fluhr, J. W. & Bos, J. D. Natural moisturizing factor components in the stratum corneum as biomarkers of filaggrin genotype: evaluation of minimally invasive methods. *Br. J. Dermatol.* **161,** 1098–1104 (2009).

54. Williamson, P. & Kligman, A. M. A new method for the quantitative investigation of cutaneous bacteria. *J. Invest. Dermatol.* **45,** 498–503 (1965).

55. Pachtman, E. A., Vicher, E. E. & Brunner, M. J. The bacteriologic flora in seborrheic dermatitis. *J. Invest. Dermatol.* **22,** 389–396 (1954).

56. Miller, C. S., Baker, B. J., Thomas, B. C., Singer, S. W. & Banfield, J. F. EMIRGE: reconstruction of full-length ribosomal genes from microbial community short read sequencing data. *Genome Biol.* **12,** R44 (2011).

57. Li, H. & Durbin, R. Fast and accurate short read alignment with Burrows–Wheeler transform. *Bioinformatics* **25,** 1754–1760 (2009).

58. Ong, S. H. *et al.* Species identification and profiling of complex microbial communities using shotgun Illumina sequencing of 16S rRNA amplicon sequences. *PLoS One* **8,** e60811 (2013).

59. Segata, N. *et al.* Metagenomic microbial community profiling using unique clade-specific marker genes. *Nature Methods* **9,** 811–814 (2012).

60. Chen, L. *et al.* VFDB: a reference database for bacterial virulence factors. *Nucleic Acids Res.* **33,** D325–D328 (2005).

61. Wilm, A. *et al.* LoFreq: a sequence-quality aware, ultra-sensitive variant caller for uncovering cell-population heterogeneity from high-throughput sequencing datasets. *Nucleic Acids Res.* **40,** 11189–11201 (2012).

62. Dickson, M. A. *et al.* Human keratinocytes that express hTERT and also bypass a p16(INK4a)-enforced mechanism that limits life span become immortal yet retain normal growth and differentiation characteristics. *Mol. Cell. Biol.* **20,** 1436–1447 (2000).

63. Malinarich, F. *et al.* High mitochondrial respiration and glycolytic capacity represent a metabolic phenotype of human tolerogenic dendritic cells. *J. Immunol.* **194,** 5174–5186 (2015).

64. Haniffa, M. *et al.* Human tissues contain CD141^{hi} cross-presenting dendritic cells with functional homology to mouse CD103^{+} nonlymphoid dendritic cells. *Immunity* **37,** 60–73 (2012).

65. Ginhoux, F. *et al.* Blood-derived dermal langerin^{+} dendritic cells survey the skin in the steady state. *J. Exp. Med.* **204,** 3133–3146 (2007).

66. Hong, C. *et al.* PathoScope 2.0: a complete computational framework for strain identification in environmental or clinical sequencing samples. *Microbiome* **2,** 33 (2014).

67. Langmead, B. & Salzberg, S. L. Fast gapped-read alignment with Bowtie 2. *Nature Methods* **9,** 357–359 (2012).

68. Abubucker, S. *et al.* Metabolic reconstruction for metagenomic data and its application to the human microbiome. *PLoS Comput. Biol.* **8,** e1002358 (2012).

69. Segata, N. *et al.* Metagenomic biomarker discovery and explanation. *Genome Biol.* **12,** R60 (2011).

Acknowledgements

Author contributions

K.R.C., M.B.Y.T., F.T.C., J.E.A.C. and N.N. planned the study. A.S.L.T., A.H.Q.N., J.W., N.M., B.J., X.F.C.C.W. and B.V.A. designed and conducted all experiments under the guidance of J.E.A.C., K.R.C., P.F.D.S., F.G. and J.E.C. Metagenomic data analysis was performed by K.R.C. and C.L. with supervision from N.N. Human skin tissue samples were collected by T.C.L. and A.W. provided technical computational assistance. B.K.S., S.A.M., Y.Y.S., F.T.C. and J.E.A.C. organized volunteer recruitment and sampling. K.R.C., A.S.L.T., E.B.L., J.E.A.C. and N.N. wrote the manuscript, with input from all authors.

Additional information

Supplementary information is available online. Reprints and permissions information is available online at www.nature.com/reprints. Correspondence and requests for materials should be addressed to J.E.A.C. and N.N.

Competing interests

The authors declare no competing financial interests.